Supplement of

The shifting of secondary inorganic aerosols formation mechanism during haze aggravation: The decisive role of aerosol liquid water

Fei Xie[1, 2], Yue Su[1, 3], Yongli Tian[2], Yanju Shi[2], Xingjun Zhou[2], Peng Wang[2], Ruihong Yu[1], Wei Wang[1], Jiang He[1, 3], Jinyuan Xin[4, *], Changwei Lü[1, 3, *]

[1] *School of Ecology and Environment, Inner Mongolia University, 010021, Hohhot, China*

[2] *Inner Mongolia Environmental Monitoring Center, 010011, Hohhot, China*

[3] *Institute of Environmental Geology, Inner Mongolia University, 010021, Hohhot, China*

[4]*State Key Laboratory of Atmospheric Boundary Layer Physics and Atmospheric Chemistry (LAPC), Institute of Atmospheric Physics, Chinese Academy of Sciences, Beijing 100029, China*

S1 Sampling and Experiment Methods

S1.1 Data acquisition and analysis methods

S1.1.1 Water-soluble inorganic ions collection and analysis

On-line ion-chromatograph instrument (MARGA ADI 2080, Metrohm Applikon, Switzerland) was employed to simultaneous acquire 9 particulate water-soluble inorganic ions species (Na^+, NH_4^+, Mg^{2+}, Ca^{2+}, K^+, Cl^-, F^-, SO_4^{2-}, NO_3^-) as well as 5 categories of corresponding trace gases (SO_2, HNO_2, HNO_3, HCl, NH_3). This instrument has already been precisely reported by numbers of work elsewhere (Rumsey et al., 2014; Nie et al., 2015; Huang et al., 2020). Briefly, wet rotary denuder (WRD) and steam jet aerosol collector (SJAC) composed of the sampling unit to collect the corresponding trace gases and aerosol samples, respectively. In detail, 10 ppm H_2O_2 filled WRD were used to absorb the gaseous pollutants (e.g., HF, HCl, HNO_3, HONO, SO_2, NH_3), while particulate species (e.g., F^-, Cl^-, NO_3^-, SO_4^{2-}, NH_4^+, Na^+, K^+, Mg^{2+}, Ca^{2+}) were collected by SJAC. By synchronizing occupying atmospheric sampling speed of 16.7L/min and WRD rotation speed of ⩾8rpm, the absorption efficiency of whole instrument reached greater than 99.7%, which makes the samples are reliable. Then, both gaseous and particulate samples are simultaneously transferred as liquid (aqueous) samples and analyzed by ion chromatography. An internal calibration standard containing Li^+ and Br^- with 1h-resolution was simultaneously injected with sample to account for any changes in the system. In addition, external standard solutions were also used to ensure perk identification and data quality. The detection limits of the particulate analytes were 0.001μg/m^3, 0.005μg/m^3, 0.004μg/m^3, 0.005μg/m^3, 0.005μg/m^3, 0.009μg/m^3, 0.006μg/m^3, 0.009μg/m^3 for Cl^-, NO_3^-, SO_4^{2-}, NH_4^+, Na^+, K^+, Mg^{2+}, Ca^{2+}, respectively. Gaseous analytes detection limits were

* Corresponding author, Email: xjy@mail.iap.ac.cn; lcw2008@imu.edu.cn

0.001μg/m^3, 0.005μg/m^3, 0.002μg/m^3, 0.003μg/m^3, 0.005μg/m^3 for HCl, HNO_3, HNO_2, SO_2, NH_3, respectively.

S1.1.2 Acquisition of Meteorological and corresponding gaseous pollutants datasets

Detailed acquisition of meteorological datasets (e.g., wind speed, wind direction, RH, temperature, etc.), gaseous pollutants (e.g., NO_x, CO, PM_1, $PM_{2.5}$, PM_{10}) and equipment model could be found in our previous work (Xie et al., 2021). In addition, apart from the previously published used data, two types of newly introduced datasets, PANs and N_2O, were measured with PANs-100 (Focused Photonics Inc.) and N_2O Monitor (LSE, Monitors), respectively.

S1.1.3 Calculation of SOR, NOR, NTR, ε(NO_3^-), ε(NH_4^+) and ε(SO_4^{2-})

Generally, SIAs formation processes always govern the aggravation of haze events. Thereby, to study the driven factors of SIA formation, sulfur oxidation ratio (SOR) and nitrogen oxidation ratio (NOR) were applied as indicators of oxidation rate in this work, which calculated as SOR= n (SO_4^{2-})/ [n (SO_2) +n (SO_4^{2-})] and NOR= [n (HNO_3) +n (NO_3^-)]/ [n (HNO_3) +n (NO_3^-) +n (NO_2)], respectively. SOR and NOR were both higher than 0.1 in this work suggesting the significant contributions of secondary transformation during the haze events (Fig. 3) (Song et al., 2007; Zhou et al., 2018). As an indicator of ammonia conversion efficient, ammonia conversion ratio (NTR), was also introduced in this work, which calculated as $NTR = (NH_4^+/18)/(NH_4^+/18 + NH_3/22.4)$. ε($NO_3^-$), ε($NH_4^+$) and ε($SO_4^{2-}$) were calculated as,$[NO_3^-]/([HNO_3] + [NO_3^-])$, $[NH_4^+]/([NH_3] + [NH_4^+])$ and $[SO_4^{2-}]/([SO_2] + [SO4_4^{2-}])$, respectively, with all the parameters being the mole concentrations.

S1.1.4 Estimate aerosol pH

Methods to infer pH based on ion balances or ratios of measured anion and cations could not act as surrogates for pH due to OH^- or H^+ could not taking into consideration (Guo et al., 2016; Guo et al., 2015). Thereby, to the best of our knowledge, the most accurate way to predict measure aerosol pH is to run a thermodynamic model on the basis of assuming the thermodynamic equilibrium. Here, ISORROPIA-II, a widely used thermodynamic model (Song et al., 2018; Gao et al., 2020) was employed in this work to establish aerosol acidity. Along with the concentrations of WSIs in $PM_{2.5}$ and gaseous pollutions (e.g., NH_3, HCl), simultaneously measured temperature and RH data were imported into its Na^+-K^+-Ca^{2+}-Mg^{2+}-NH_4^+-SO_4^{2-}-NO_3^--Cl^--H_2O aerosol system. Based on the previous study on this model (Song et al., 2018) and the our data profiles, forward mode and metastable state in this model were chosen to calculate aerosol acidity and aerosol water content. The pH was calculated by using the following equation,

$$pH = -\log_{10}\frac{1000H_{air}^+}{ALWC}$$

where ALWC and H_{air}^{+} is the aerosol liquid water content and H^{+} loading for per volume air in μg/m^3, respectively, which was calculated by ISORROPIA-II.

Extremely high correlations between measured and modeled concentrations of NH_3, NH_4^{+}, NO_3^{-} and SO_4^{2-} were observed by occupying this model, with correlation coefficient ranged from 0.971 to 0.999 and distributed around the 1:1 line, which indicated the highly accuracy of this model (Fig. S1).

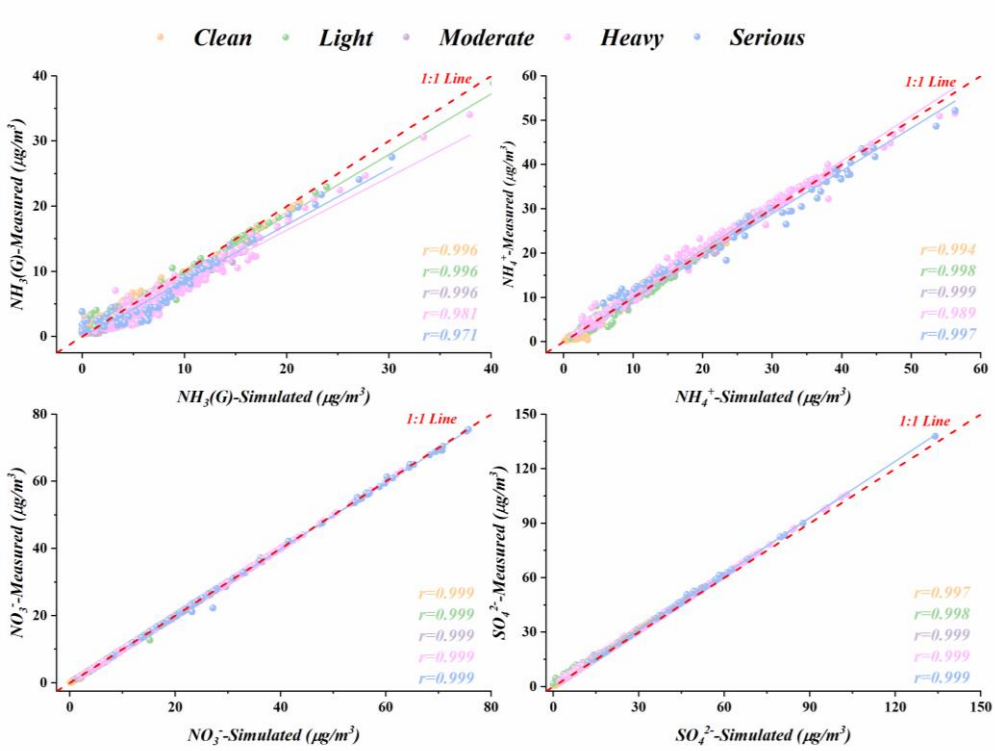

Fig. S1 Correlations of NH_3, NH_4^{+}, NO_3^{-} and SO_4^{2-} between measured and ISORROPIA-II simulated results

S2 Results and Discussion

In this work, Ministry of Ecology and Environment of the People's Republic of China established air quality index (AQI, HJ633-2012, http://www.mee.gov.cn/) was introduced. Detailed calculation processes and cut-point could be found in previous works (Kanchan et al., 2015; Xu et al., 2017). Briefly, daily concentrations of $PM_{2.5}$ ranged from 0-75, 75-115, 115-150, 150-250 and >250 μg/m^3 were classified as clean (C), light polluted (L), moderate polluted (M), heavy polluted (H) and serious polluted (S) periods, respectively.

S2.1 In-situ high-resolution observations

The average concentrations of PM_{10}, $PM_{2.5}$, $PM_{1.0}$ were 108.5±68.3, 84.75±84.5, 63.18±96.0 μg/m^3, respectively, with a wide range of variability due to several haze events occurred during

the studied period (Fig. S2). It was notable that SO_2 was maintained at a relatively low level (18.97±15.0 μg/m^3) since the implementation of pollution controlling policy in recent years, compared with the neighboring city in 2014 (Zhou et al., 2018) and its own SO_2 concentration during 2014 (50 μg/m^3). Whereas, concentrations of other reactive precursors were basically maintained at relative high level, such as NO_2 (44.56±18.6 μg/m^3), NH_3 (5.55±4.07 μg/m^3), compared with 2014 (Yearly average NO_2 concentration, 44 μg/m^3). Meanwhile, as a typical tracer of combustion, significantly elevated CO emphasized contributions of incomplete combustion on haze intensification. In addition, O_3 was the only significantly declined pollutant with the haze aggravation, due to the weakened solar radiation led by the aggravated haze, which indicating significantly reduces the SIA formation processes through the oxidation between gaseous precursors, OH radicals and stabilized Criegee intermediate (sCI) by considering the determining role of O_3 in the formation of OH radicals and sCI in the atmosphere (Mauldin Iii et al., 2012; Hua et al., 2008). As for meteorological conditions, low temperature and high humidity were observed during the studied period, with the values were -8.45±4.42 °C and 65.59±14.07 %, respectively.

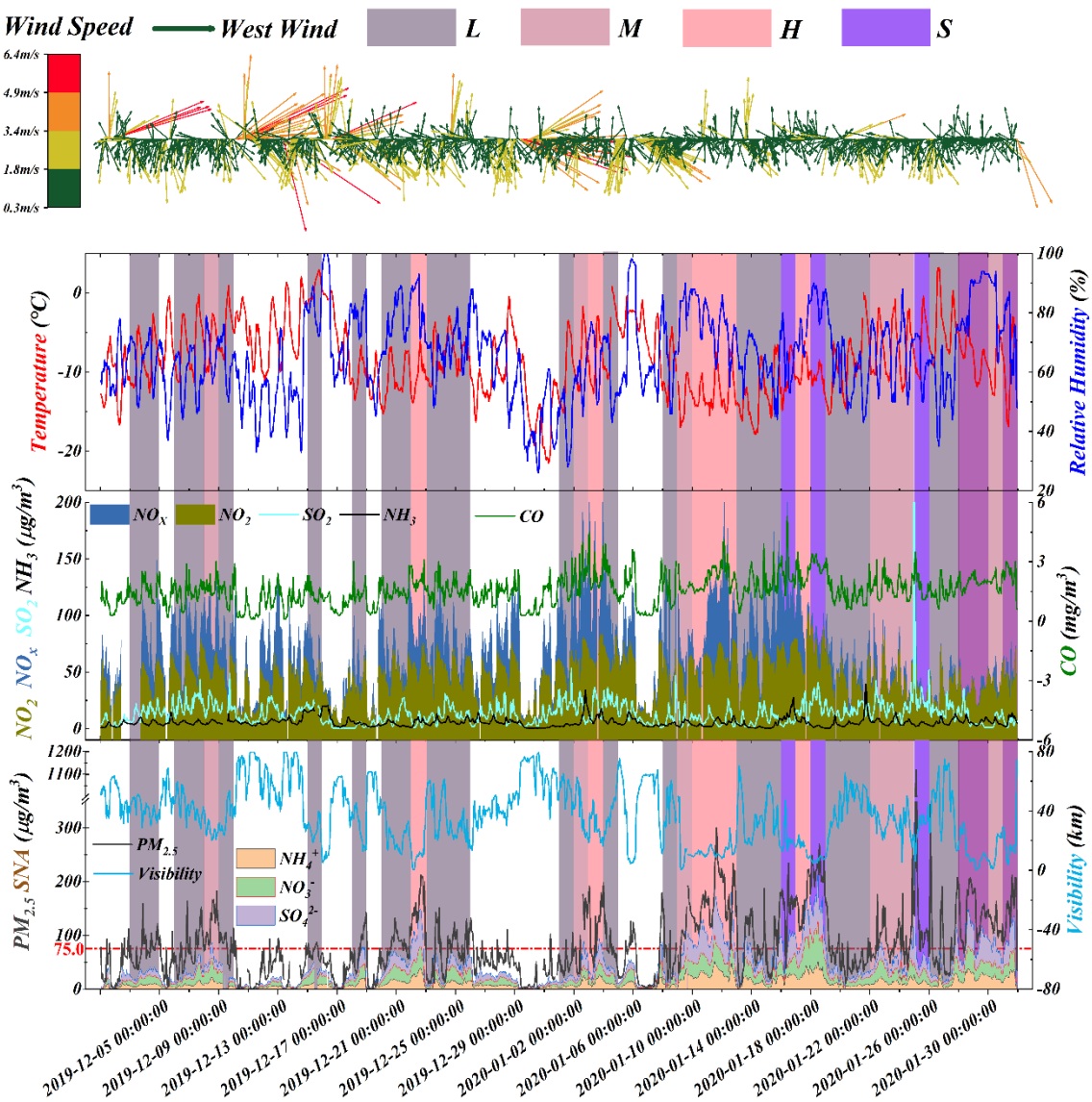

Fig. S2 Time series of meteorological conditions and atmospheric pollutants

$PM_{2.5}$ concentrations presented increasing trends with pollution levels (Fig. S3), and its pH ranged from 0.63 to 6.32 (calculated by ISORROPIA-II), mainly concentrated at 4~5 (Fig. S4). The weak acidic nature of particles was consistent with Tianjin, China (Gao et al., 2020). With the worsening of the haze events, the average concentrations of gaseous precursors, such as SO_2, NO_x, NH_3, were 2.27, 1.33, 1.26 times of those in clean periods, respectively, indicating the increasingly enhanced importance of precursors on SIA generations. Additionally, it was notable that along with haze aggravation, SIA consecutively sharing the most abundant species in $PM_{2.5}$ and all detected ions, highlighting the determining role of SIA on regional haze aggravation and consistent with previous works (Fig. S3) (Xu et al., 2017; Gao et al., 2020; Huang et al., 2020). Meanwhile, the stabilized conditions, characterized by gradually lower wind speed (from 1.79±1.2 to 1.15±0.47 m/s) and higher RH (from 59.48±15.0 to

71.13±11.9 %) during haze events, further aggravating the regional haze by hindering the diffusion of particulates and accelerating its hygroscopic growth (Tab. S1) (Zhang et al., 2009; Zheng et al., 2015; Zhang et al., 2015; Yang et al., 2015).

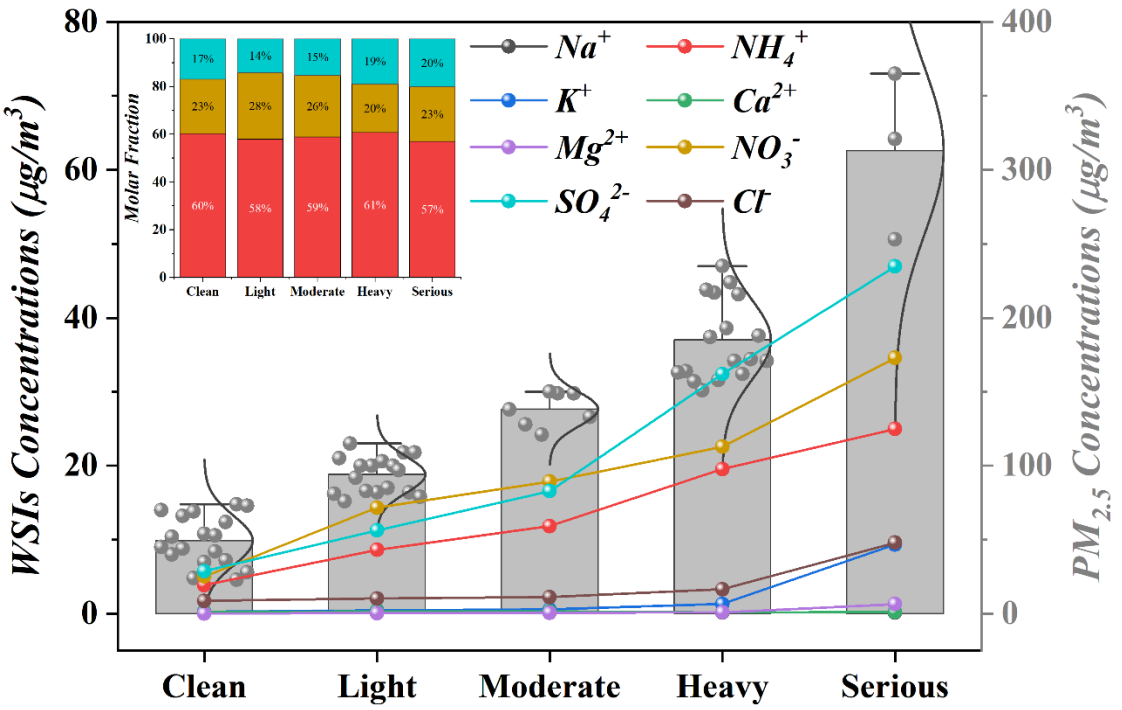

Fig. S3 Characteristics of WSIs under various pollution periods

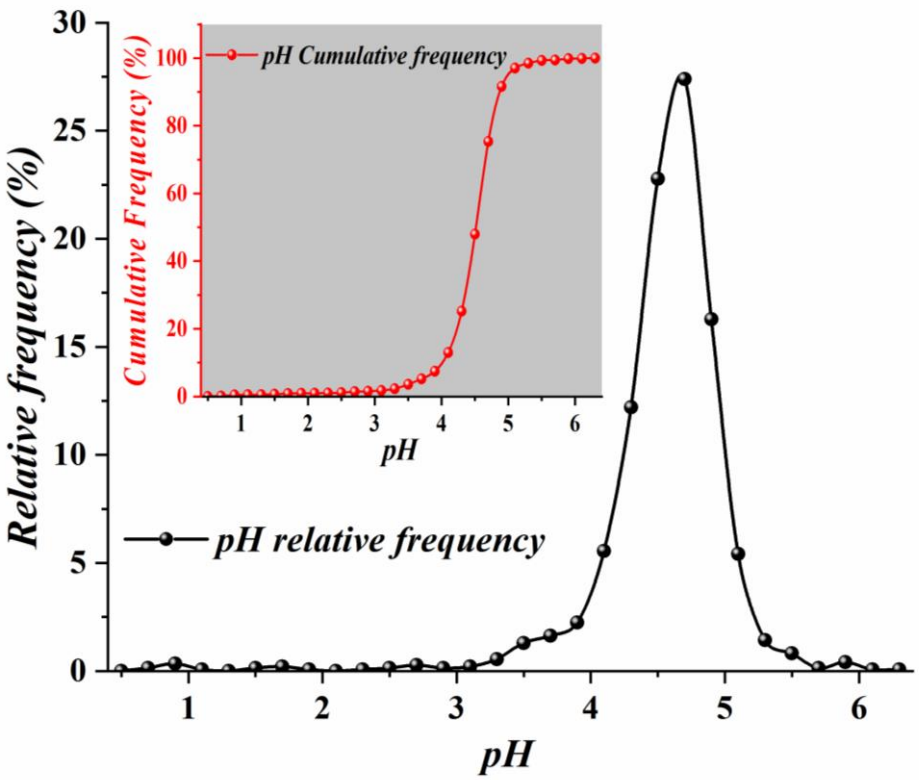

Fig. S4 pH distribution frequency during the studied campaign

S 2.2 Chemical forms of ammonium species

Although anions could react with primary ions to generate non-volatile compounds, the mass fractions of primary ions to total ions only less than 5.2% and neglected in this work. Thus, molar ratios of NH_4^+ vs. anions could be treated as indicators to identify the chemical forms of ammonium salts guided by stoichiometry (Zhou et al., 2018; Wang et al., 2021; Liu et al., 2017). Briefly, NH_3 prefer react with H_2SO_4 to form non-volatile NH_4HSO_4 or $(NH_4)_2SO_4$ under NH_4^+-poor conditions, afterwards, semi-volatile NH_4NO_3 and NH_4Cl would subsequently generate by existing sufficient NH_3 through neutralize atmospheric HNO_3 and HCl. Roughly, average molar fractions of NH_4^+ accounting for nearly four times of sulfate molar concentrations throughout the studied periods (Fig. S3), indicating the atmospheric SO_4^{2-} were completely neutralized by NH_4^+ and formed ammonium sulfate and ammonia bisulfate according to the stoichiometry results between NH_4^+ and sulfate (Zhou et al., 2018; Wang et al., 2021; Liu et al., 2017). Detailly, according to Fig. S5a, significant correlations between n (NH_4^+) and n (SO_4^{2-}) with correlation coefficient of 0.947 and slope much lower than 0.5 further highlighting the atmospheric SO_4^{2-} completely neutralized by NH_4^+ to yield ammonium sulfate and ammonia bisulfate. To further explore the chemical forms of the remaining ammonium, the concept of "excess NH_4^+", which calculated as $[NH_4^+]-1.5\times[SO_4^{2-}]$ in molar concentration (Shi et al., 2019), was introduced to explore the chemical species of excess NH_4^+. The correlations between n (excess NH_4^+) and n(NO_3^-) (Fig. S5b) suggested that atmospheric NH_4^+ not only enough to neutralize both SO_4^{2-} and NO_3^- forming two major species of $(NH_4)_2SO_4$ and NH_4NO_3 during any pollution stage, but also remained on particles as free NH_4^+. The particulate residual NH_4^+ were further confirmed by gas ratio (GR) >1 (Fig. S6) on the basis of GR >1 indicating NH_4NO_3 formation is limited by the availability of HNO_3 (Paulot et al., 2016). Besides, starting with light pollution periods, the scatters of n (excess NH_4^+) and n ($Cl^-+NO_3^-$) gradually moves from above 1:1 line to below 1:1 line, indicating the coexistence of particle NH_4NO_3 and NH_4Cl and increasingly ammonium ionized on particulate matter from this period (Fig.S5c). Additionally, the remaining ammonium, as well as other detected alkalic cations, may react with undetected CO_3^{2-}, HCO_3^- and organic materials (e.g., water-soluble organic acids, sugars, alcohols, etc.) through complexation reaction and form metal coordination compounds (Nozière et al., 2010; Chang-Graham et al., 2011; Cui et al., 2021). Therefore, the predominant chemical domains of ammonium species gradually transited from the predominance of ammonium sulfate and ammonium nitrate during clean periods to the coexistence of ammonium sulfate, ammonium nitrate and ammonium chloride.

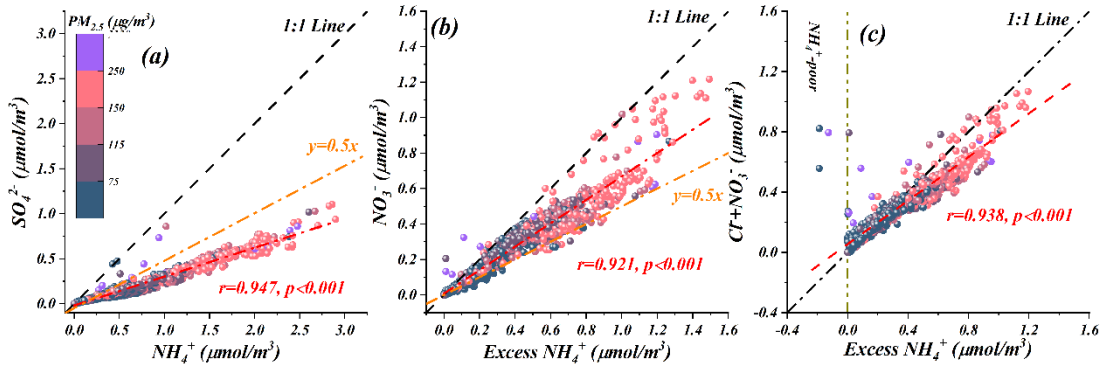

Fig. S5 Correlations between NH_4^+ and water-soluble anions among various pollution periods

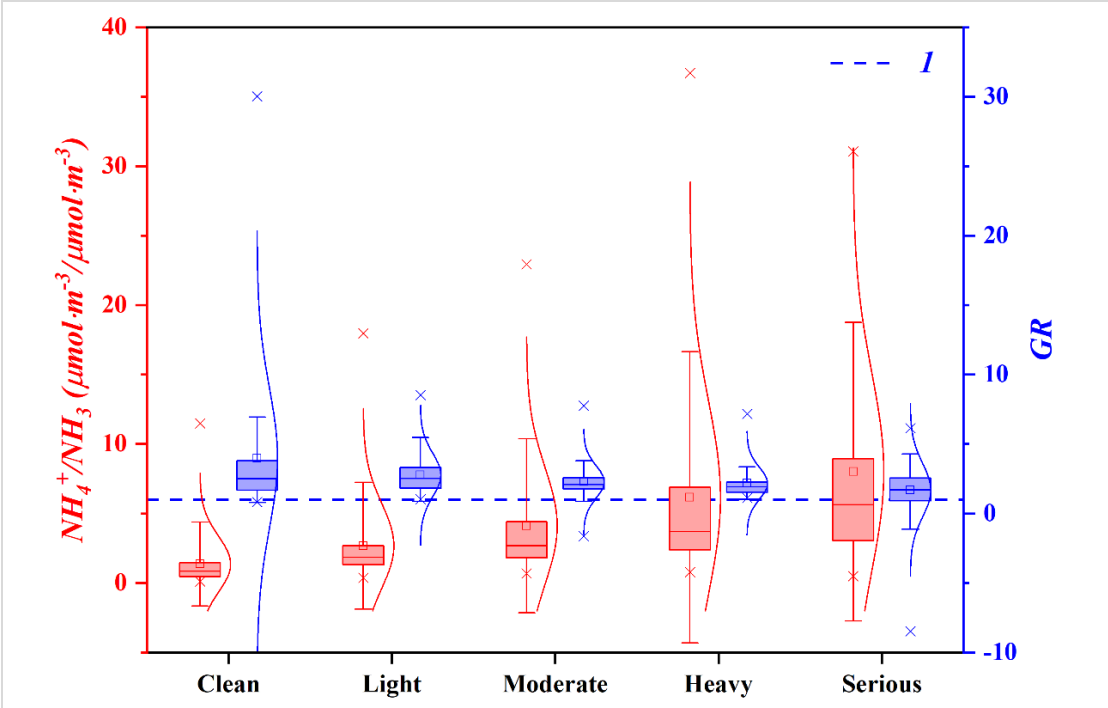

Fig. S6 Box-type of NH_4^+/NH_3 and gas ratio (GR)

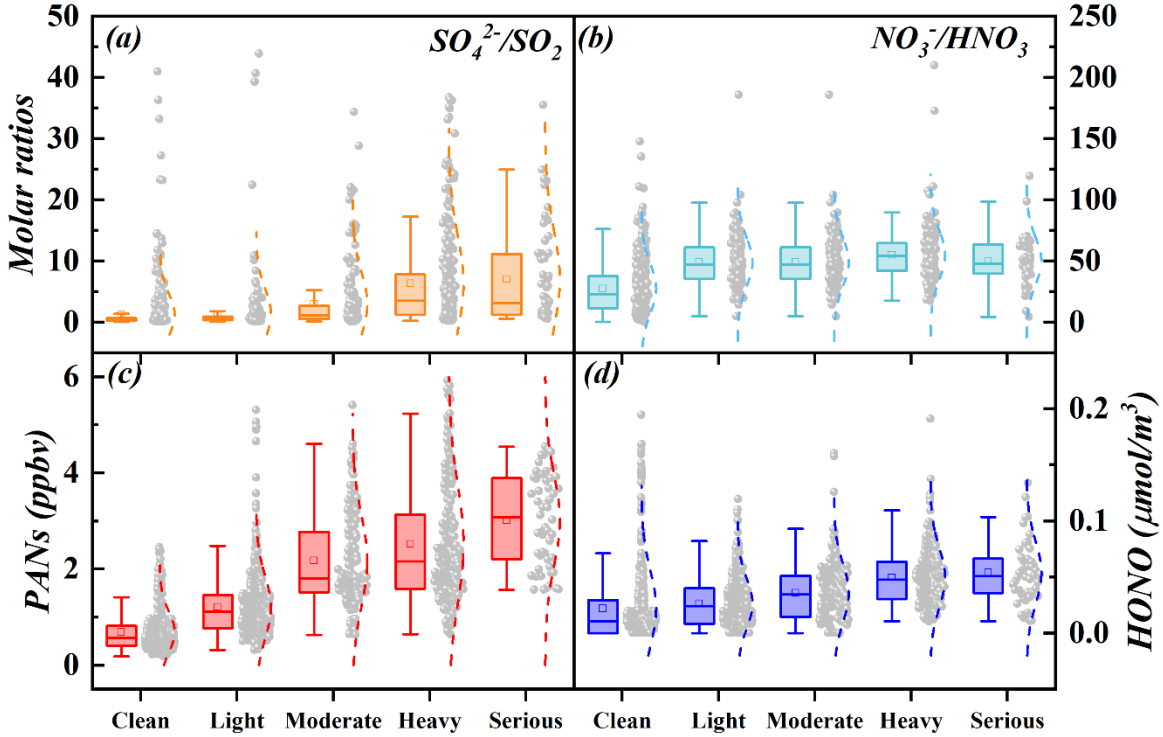

Fig. S7 Box-type of (a) SO_4^{2-}/SO_2, (b)NO_3^-/HNO_3, (c)PANs and (d)HONO response to different pollution stages

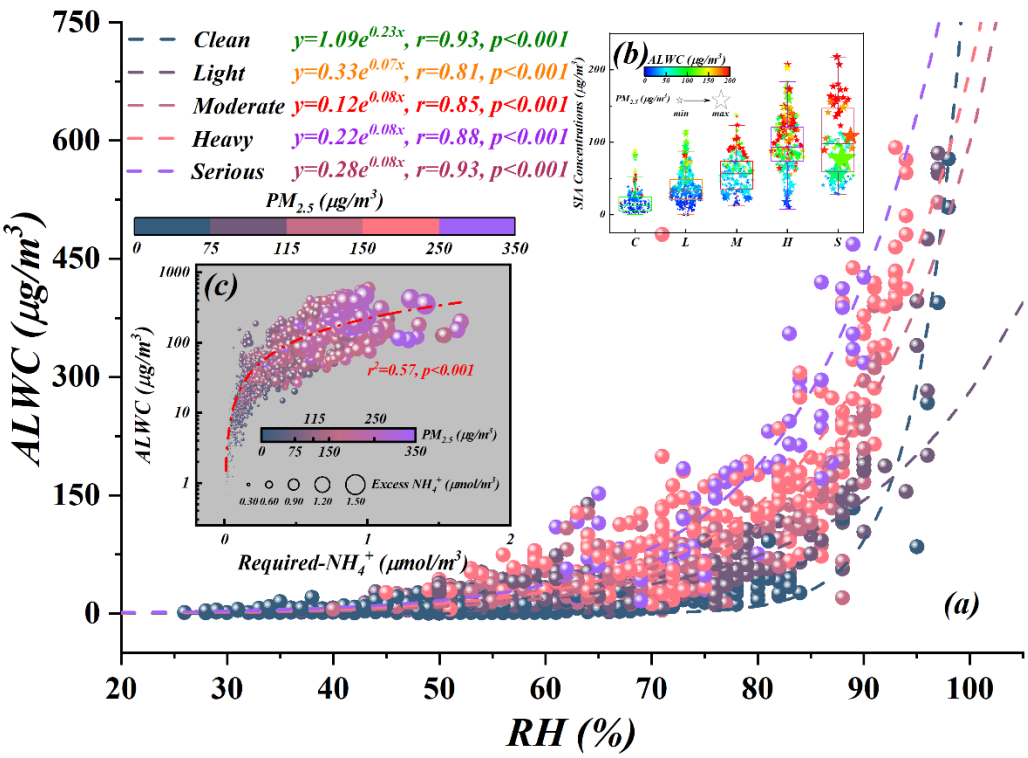

Fig. S8 (a)Correlations of $PM_{2.5}$ concentrations and ALWC with different pollution stages, (b) SIA mass fractions in

PM2.5 during entire periods. The pentagrams were colored as a function of aerosol liquid water content, and the size of pentagrams corresponding to the PM2.5 mass concentrations, (c) Correlations between Required- NH_4^+ and ALWC corresponding to $PM_{2.5}$ and excess-NH_4^+, required NH_4^+ and excessNH_4^+ were calculated according to the formula in S.M. text S2

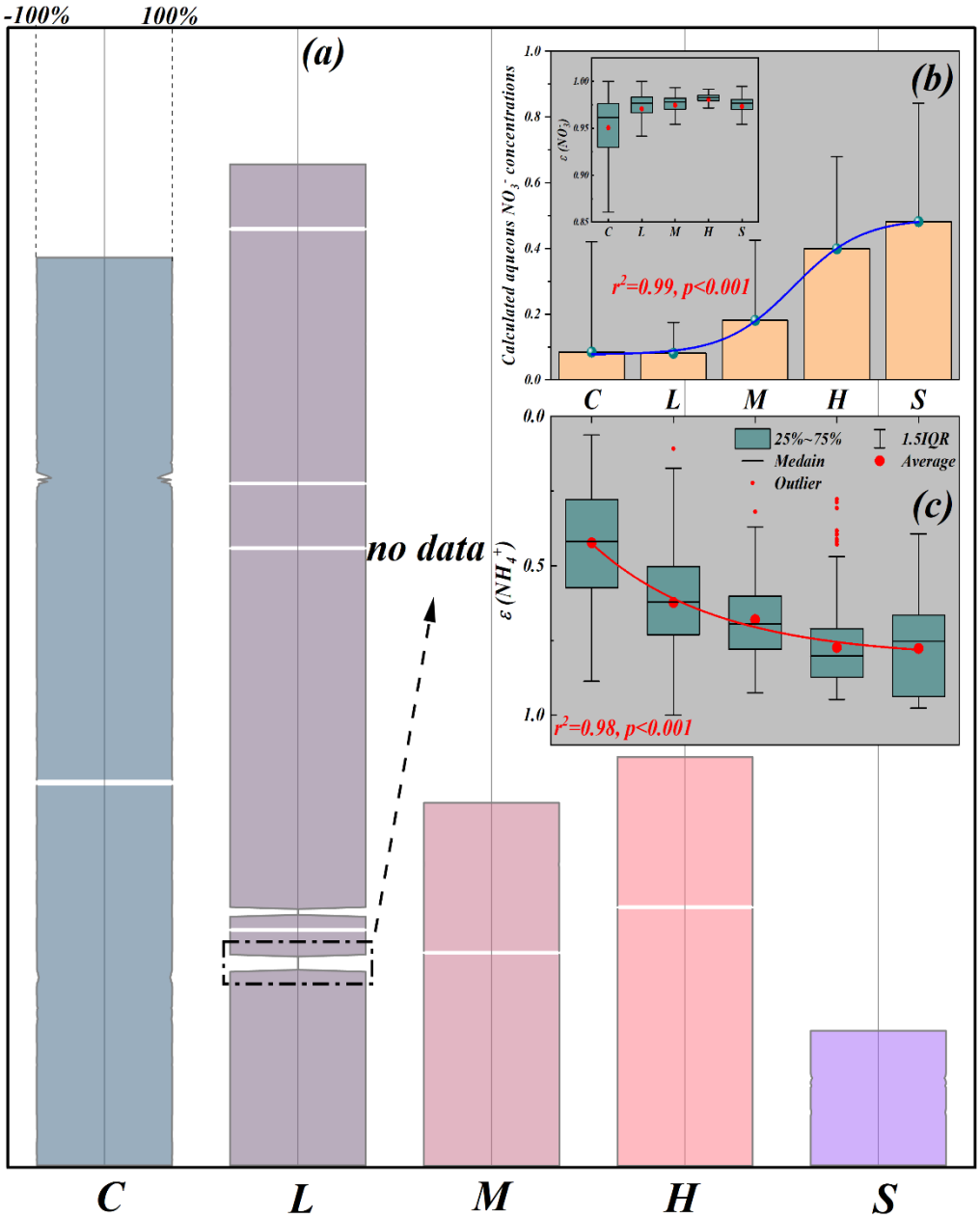

Fig. S9 (a) Statistics of time series of nitrate loading capacity response to different pollution stages, (c) statistics of ε(NH_4^+) response to different pollution stages, (b) calculated aqueous-NO_3^- concentrations and ε(NO_3^-) corresponding to pollution stages, the calculation processes followed by Guo et al. (2015); Guo et al. (2016); Guo et al. (2017)

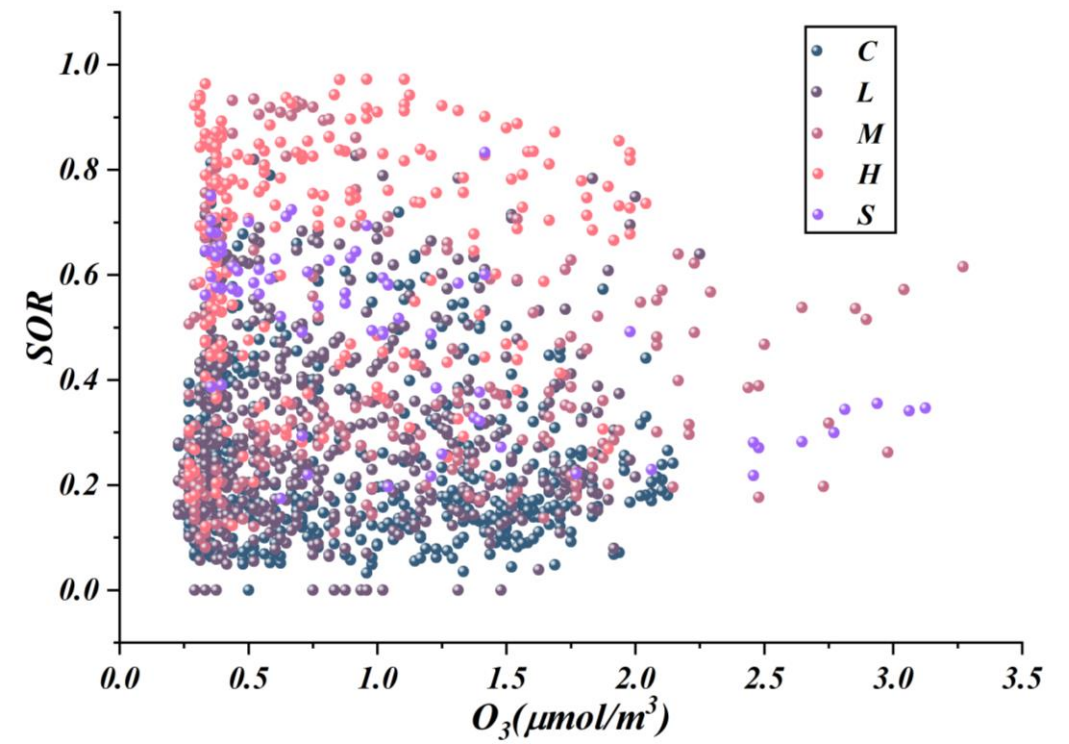

Fig. S10 Correlations between O_3 and SOR response to different pollution stages

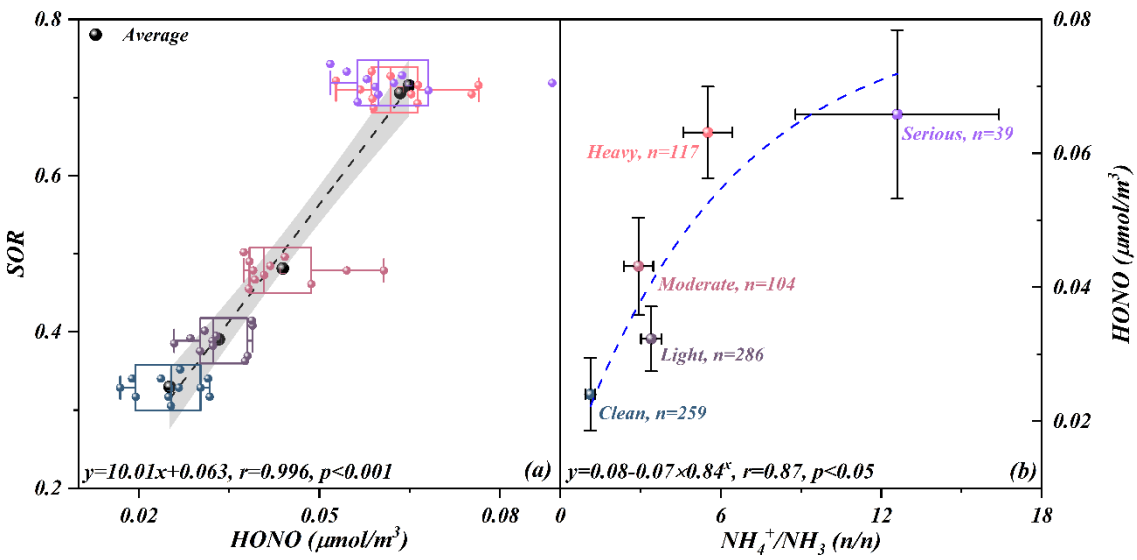

Fig. S11 Correlations between (a) HONO and SOR, (b) NH_4^+/NH_3 and HONO response to different pollution stages. To minimize the dependences mixed layer depth during diurnal changes and avoid the fast photolysis of HONO in the daytime, the nighttime hours were selected and corresponding to 20:00-7:00

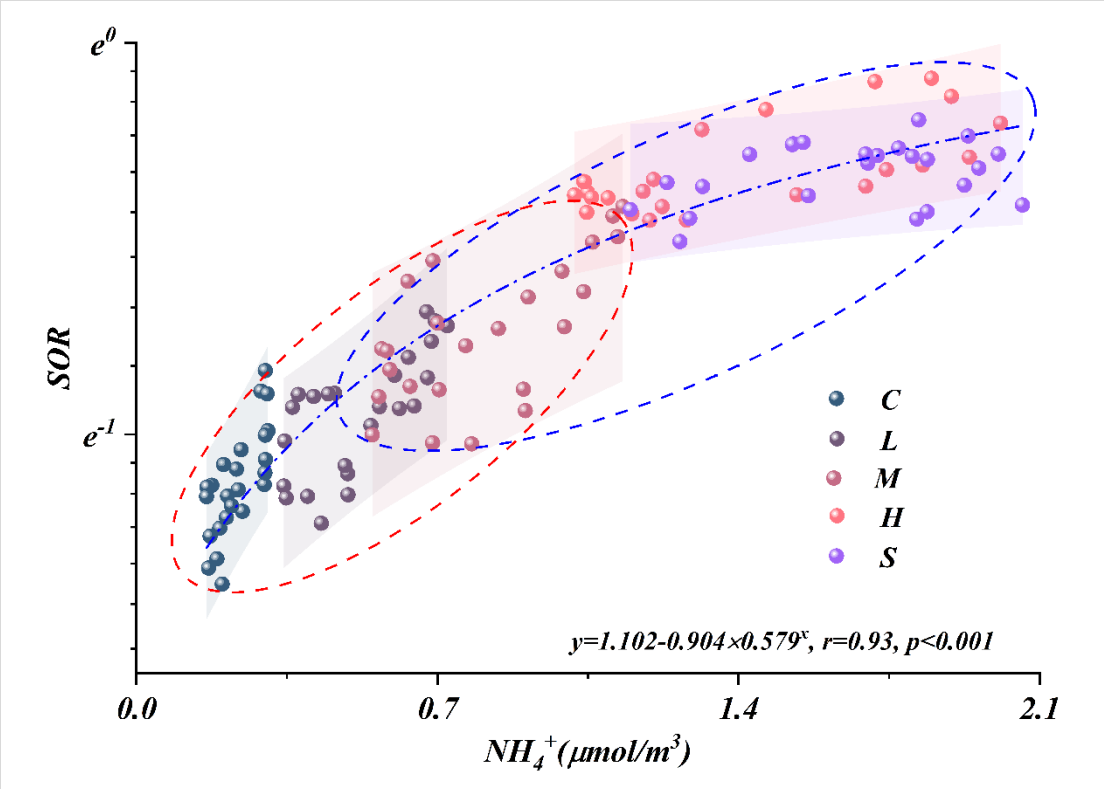

Fig. S12 Correlations between NH_4^+ and SOR response to different pollution stages

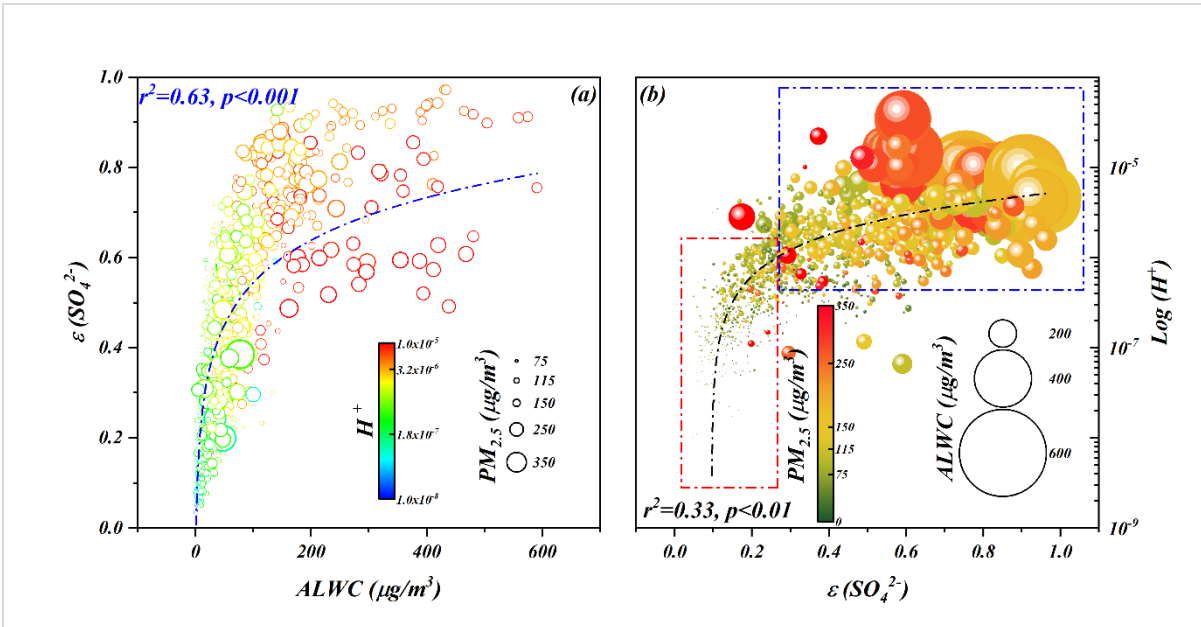

Fig. S13 (a) correlations between ALWC and $\varepsilon(SO_4^{2-})$ corresponding to H^+ and $PM_{2.5}$, (b) correlations between $\varepsilon(SO_4^{2-})$ and $\log(H^+)$ corresponding to $PM_{2.5}$ and ALWC

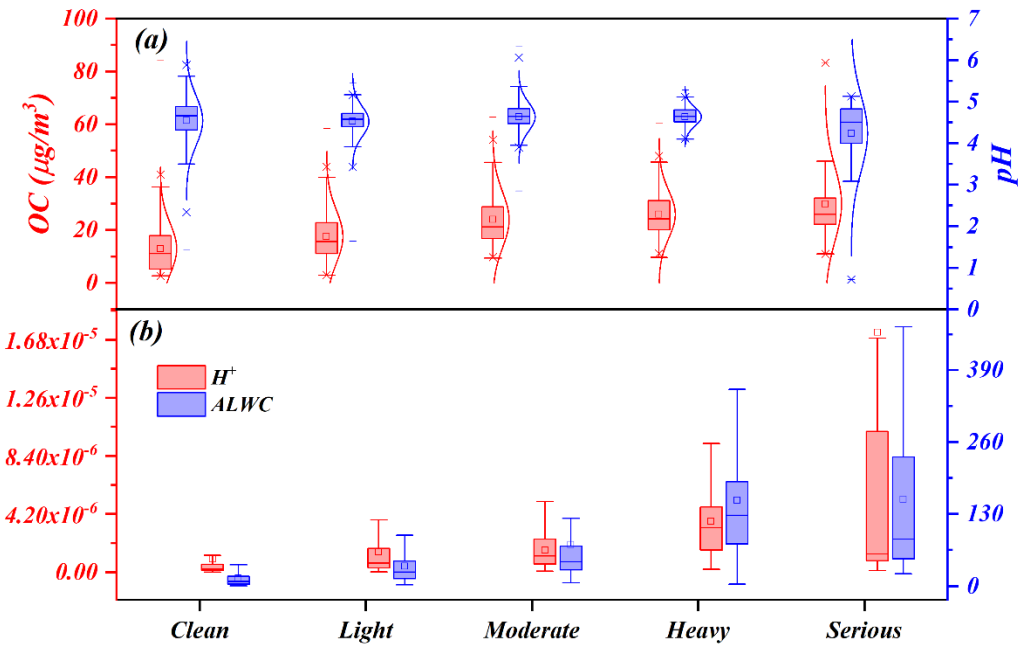

Fig. S14 Box-type of (a) OC and pH, (b) H^+ and ALWC corresponding to different pollution stages

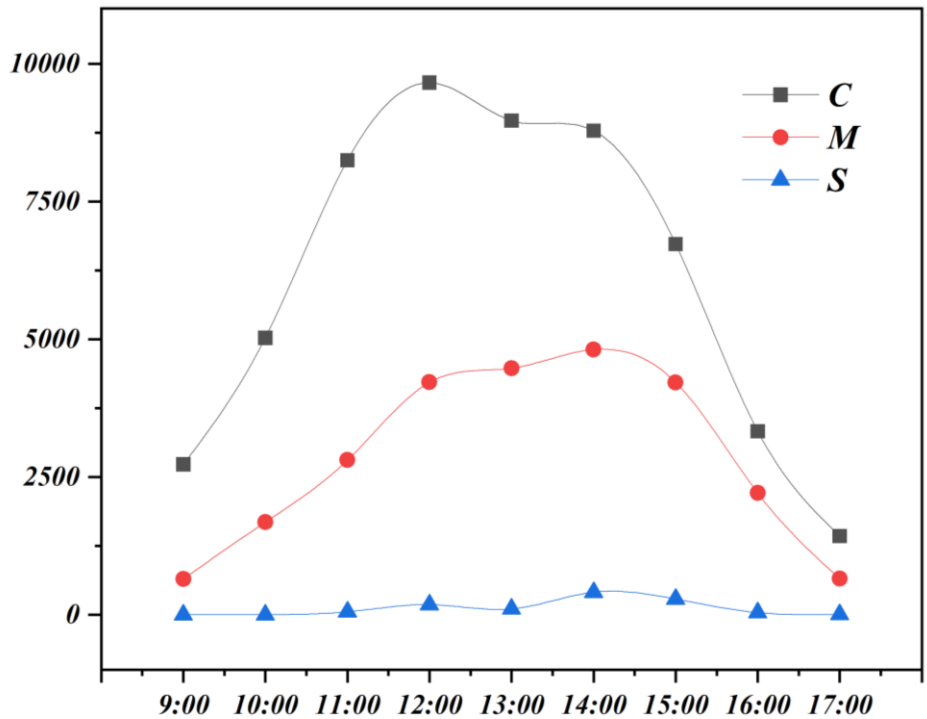

Fig. S15 Diurnal solar spectrophotometry at 380 nm at clean and moderate pollution stages

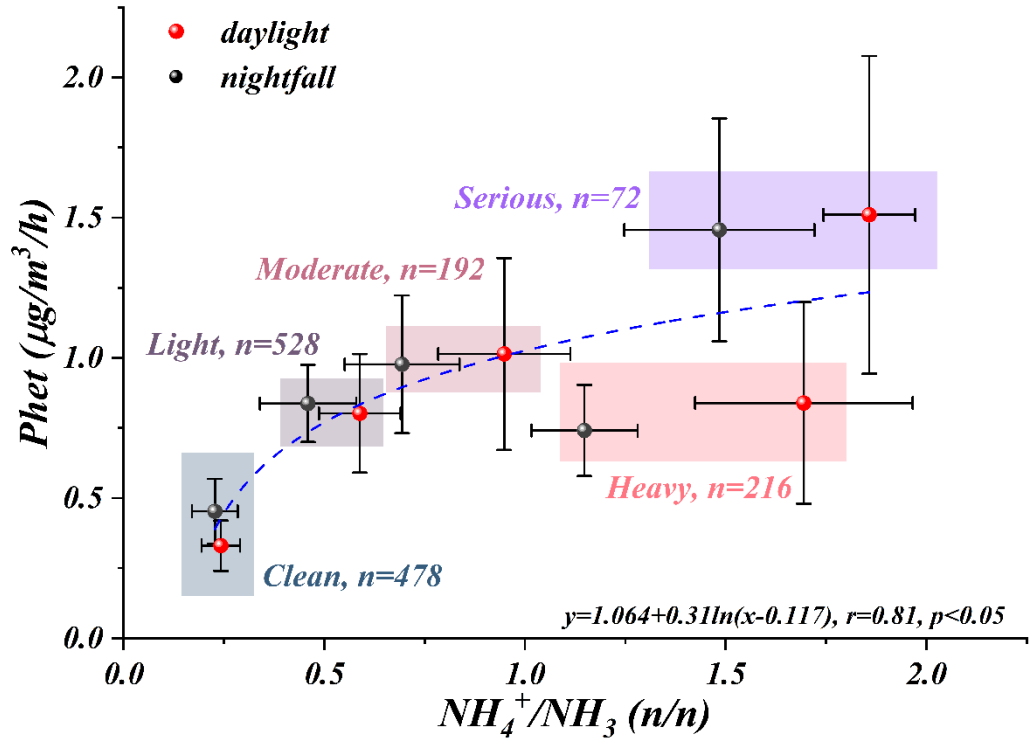

Fig. S16 Correlations between calculated P_{het} and ammonium partitioning corresponding to different pollution stages

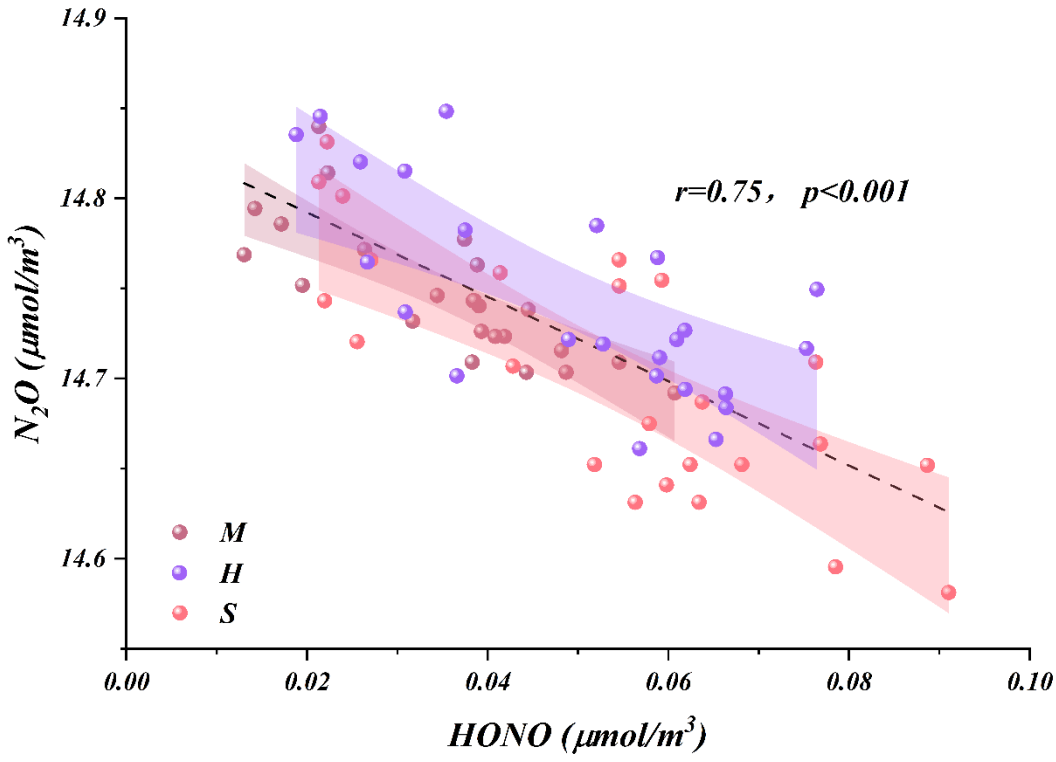

Fig. S17 Correlations between HONO and N_2O corresponding to pollution stages

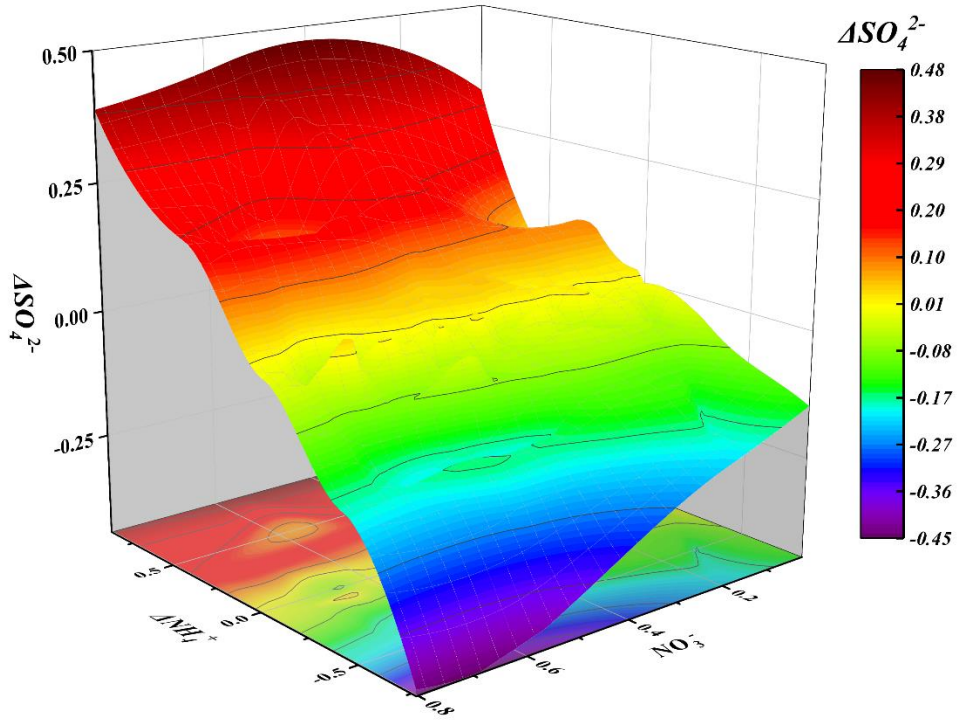

Fig. S18 Observation of inhibition and promotion of sulfate production by nitrate and ammonium, respectively. All data were matrixed to avoid interference caused by dimensionality

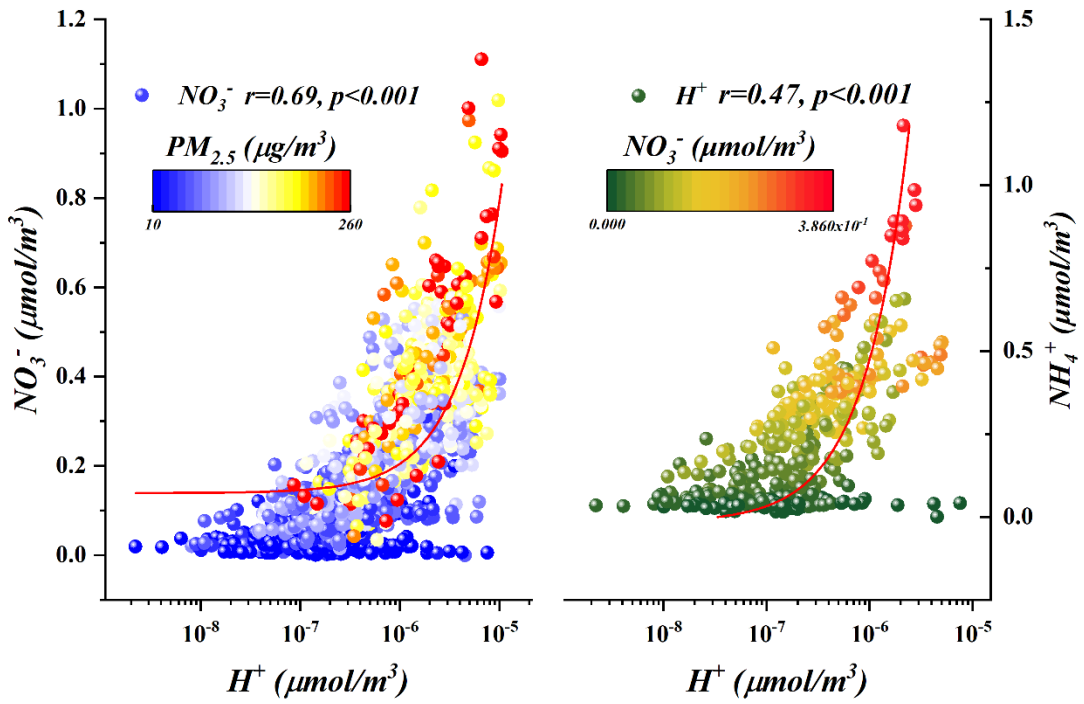

Fig. S19 Correlations between (a) H^+ and NO_3^- corresponding to $PM_{2.5}$ concentrations, (b) H^+ and NH_4^+ corresponding to NO_3^- molar concentrations

Table S1 Description of meteorological parameters and atmospheric pollutants

	Whole Campaign	*Clean*	*Light*	*Moderate*	*Heavy*	*Serious*
Temperature (°C)	-8.45±4.42	-7.92±5.0	-8.42±4.4	-7.73±4.0	-10.08±3.2	-9.13±3.3
RH (%)	65.59±14.1	59.48±15.0	64.64±11.7	68.33±12.5	77.27±10.3	71.13±11.9
Wind Speed (m/s)	1.43±0.87	1.79±1.2	1.25±0.6	1.07±0.5	1.01±0.5	1.15±0.47
Visibility (km)	37.50±20.4	52.36±18.1	38.12±14.1	30.77±20.3	15.01±10.0	18.98±11.7
Solar Radiation (w/m^2)	82.09±135.9	81.31±136.8	83.73±137.7	80.35±144.1	75.7±125.84	73.32±124.7
O_3 ($\mu g/m^3$)	43.41±27.4	45.29±26.5	38.79±22.9	54.23±35.3	38.71±24.3	30.94±14.3
NO_2 ($\mu g/m^3$)	44.56±18.6	35.72±19.8	45.18±16.4	47.40±14.8	51.99±17.6	57.10±21.1
NO_x ($\mu g/m^3$)	65.62±35.2	51.65±32.5	69.91±29.3	63.58±34.3	82.03±41.0	80.93±40.0
SO_2 ($\mu g/m^3$)	18.97±15.0	14.59±10.2	21.72±11.1	21.52±11.8	15.01±11.1	33.08±43.4
CO (mg/m^3)	1.57±0.75	1.06±0.66	1.58±0.6	1.82±0.6	2.18±0.6	2.40±0.8
NH_3 ($\mu g/m^3$)	5.55±4.07	5.08±3.84	5.24±3.96	6.31±4.43	6.37±3.37	6.42±6.09
PM_1 ($\mu g/m^3$)	63.18±96.0	32.02±23.2	55.27±25.4	86.16±143.9	90.47±27.7	170.7±316.7
$PM_{2.5}$ ($\mu g/m^3$)	84.75±84.5	39.11±31.1	71.21±35.9	112.38±144.6	150.10±46.0	192.14±162.9
PM_{10} ($\mu g/m^3$)	108.5±68.3	63.05±42.8	98.95±45.8	128.77±58.8	177.55±53.2	200.97±114.6
PM_1 /$PM_{2.5}$	0.84±0.39	0.87±0.08	0.92±0.06	0.94±0.02	0.95±0.02	0.96±0.01
$PM_{2.5}$ /PM_{10}	0.71±0.19	0.73±0.15	0.84±0.11	0.89±0.06	0.93±0.05	0.93±0.04
pH	4.54±0.51	4.54±0.59	4.52±0.35	4.63±0.34	4.64±0.22	4.16±1.26

Notes: all datasets were presented as mean± S.D.

References:

Technical Regulation on Ambient Air Quality Index (on trail) (HJ633-2012), Ministry of Ecology and Environment of the People's Republic of China,

Chang-Graham, A. L., Profeta, L. T. M., Johnson, T. J., Yokelson, R. J., Laskin, A., and Laskin, J.: Case Study of Water-Soluble Metal Containing Organic Constituents of Biomass Burning Aerosol, Environ. Sci. Technol., 45, 1257-1263, 10.1021/es103010j, 2011.

Cui, Y., Frie, A. L., Dingle, J. H., Zimmerman, S., Frausto-Vicencio, I., Hopkins, F., and Bahreini, R.: Influence of Ammonia and Relative Humidity on the Formation and Composition of Secondary Brown Carbon from Oxidation of 1-Methylnaphthalene and Longifolene, ACS Earth and Space Chem., 5, 858-869, 10.1021/acsearthspacechem.0c00353, 2021.

Gao, J., Wei, Y., Shi, G., Yu, H., Zhang, Z., Song, S., Wang, W., Liang, D., and Feng, Y.: Roles of RH, aerosol pH and sources in concentrations of secondary inorganic aerosols, during different pollution periods, Atmos. Environ., 241, 117770, https://doi.org/10.1016/j.atmosenv.2020.117770, 2020.

Guo, H., Liu, J., Froyd, K. D., Roberts, J. M., Veres, P. R., Hayes, P. L., Jimenez, J. L., Nenes, A., and Weber, R. J.: Fine particle pH and gas–particle phase partitioning of inorganic species in Pasadena, California, during the 2010 CalNex campaign, Atmos. Chem. Phys., 17, 5703-5719, 10.5194/acp-17-5703-2017, 2017.

Guo, H., Sullivan, A. P., Campuzano-Jost, P., Schroder, J. C., Lopez-Hilfiker, F. D., Dibb, J. E., Jimenez, J. L., Thornton, J. A., Brown, S. S., Nenes, A., and Weber, R. J.: Fine particle pH and the partitioning of nitric acid during winter in the northeastern United States, J. Geophys. Res.: Atmospheres, 121, 10,355-310,376, https://doi.org/10.1002/2016JD025311, 2016.

Guo, H., Xu, L., Bougiatioti, A., Cerully, K. M., Capps, S. L., Hite Jr, J. R., Carlton, A. G., Lee, S. H., Bergin, M. H., Ng, N. L., Nenes, A., and Weber, R. J.: Fine-particle water and pH in the southeastern United States, Atmos. Chem. Phys., 15, 5211-5228, 10.5194/acp-15-5211-2015, 2015.

Hua, W., Chen, Z. M., Jie, C. Y., Kondo, Y., Hofzumahaus, A., Takegawa, N., Chang, C. C., Lu, K. D., Miyazaki, Y., Kita, K., Wang, H. L., Zhang, Y. H., and Hu, M.: Atmospheric hydrogen peroxide and organic hydroperoxides during PRIDE-PRD'06, China: their concentration, formation mechanism and contribution to secondary aerosols, Atmos. Chem. Phys., 8, 6755-6773, 10.5194/acp-8-6755-2008, 2008.

Huang, R.-J., Duan, J., Li, Y., Chen, Q., Chen, Y., Tang, M., Yang, L., Ni, H., Lin, C., Xu, W., Liu, Y., Chen, C., Yan, Z., Ovadnevaite, J., Ceburnis, D., Dusek, U., Cao, J., Hoffmann, T., and O'Dowd, C. D.: Effects of NH_3 and alkaline metals on the formation of particulate sulfate and nitrate in wintertime Beijing, Sci. Total Environ., 717, 137190, https://doi.org/10.1016/j.scitotenv.2020.137190, 2020.

Kanchan, K., Gorai, A. K., and Goyal, P.: A review on air quality indexing system, Asian Journal of Atmospheric Environment, 9, 101-113, 2015.

Liu, Z., Xie, Y., Hu, B., Wen, T., Xin, J., Li, X., and Wang, Y.: Size-resolved aerosol water-soluble ions during the summer and winter seasons in Beijing: Formation mechanisms of secondary inorganic aerosols, Chemosphere, 183, 119-131, https://doi.org/10.1016/j.chemosphere.2017.05.095, 2017.

Mauldin Iii, R. L., Berndt, T., Sipilä, M., Paasonen, P., Petäjä, T., Kim, S., Kurtén, T., Stratmann, F., Kerminen, V. M., and Kulmala, M.: A new atmospherically relevant oxidant of sulphur dioxide, Nature, 488, 193-196, 10.1038/nature11278, 2012.

Nie, W., Ding, A. J., Xie, Y. N., Xu, Z., Mao, H., Kerminen, V. M., Zheng, L. F., Qi, X. M., Huang, X., Yang, X. Q., Sun, J. N., Herrmann, E., Petäjä, T., Kulmala, M., and Fu, C. B.: Influence of biomass burning plumes on HONO chemistry in eastern China, Atmos. Chem. Phys., 15, 1147-1159, 10.5194/acp-15-1147-2015, 2015.

Nozière, B., Dziedzic, P., and Córdova, A.: Inorganic ammonium salts and carbonate salts are efficient catalysts for aldol condensation in atmospheric aerosols, Physical chemistry chemical physics : PCCP, 12, 3864-3872, 10.1039/b924443c, 2010.

Paulot, F., Ginoux, P., Cooke, W. F., Donner, L. J., Fan, S., Lin, M. Y., Mao, J., Naik, V., and Horowitz, L. W.: Sensitivity of nitrate aerosols to ammonia emissions and to nitrate chemistry: implications for present and future nitrate optical depth, Atmos. Chem. Phys., 16, 1459-1477, 10.5194/acp-16-1459-2016, 2016.

Rumsey, I. C., Cowen, K. A., Walker, J. T., Kelly, T. J., Hanft, E. A., Mishoe, K., Rogers, C., Proost, R., Beachley, G. M., Lear, G., Frelink, T., and Otjes, R. P.: An assessment of the performance of the Monitor for AeRosols and GAses in ambient air (MARGA): a semi-continuous method for soluble compounds, Atmos. Chem. Phys., 14, 5639-5658, 10.5194/acp-14-5639-2014, 2014.

Shi, G., Xu, J., Shi, X., Liu, B., Bi, X., Xiao, Z., Chen, K., Wen, J., Dong, S., Tian, Y., Feng, Y., Yu, H., Song, S., Zhao, Q., Gao, J., and Russell, A. G.: Aerosol pH Dynamics During Haze Periods in an Urban Environment in China: Use of Detailed, Hourly, Speciated Observations to Study the Role of Ammonia Availability and Secondary Aerosol Formation and Urban Environment, J. Geophys. Res.: Atmospheres, 124, 9730-9742, https://doi.org/10.1029/2018JD029976, 2019.

Song, C. H., Kim, C. M., Lee, Y. J., Carmichael, G. R., Lee, B. K., and Lee, D. S.: An evaluation of reaction probabilities of sulfate and nitrate precursors onto East Asian dust particles, J. Geophys. Res. Atmos., 112, D18206, https://doi.org/10.1029/2006JD008092, 2007.

Song, S., Gao, M., Xu, W., Shao, J., Shi, G., Wang, S., Wang, Y., Sun, Y., and McElroy, M. B.: Fine-particle pH for Beijing winter haze as inferred from different thermodynamic equilibrium models, Atmos. Chem. Phys., 18, 7423-7438, 10.5194/acp-18-7423-2018, 2018.

Wang, H., Wang, X., Zhou, H., Ma, H., Xie, F., Zhou, X., Fan, Q., Lü, C., and He, J.: Stoichiometric characteristics

and economic implications of water-soluble ions in $PM_{2.5}$ from a resource-dependent city, Environ. Res., 193, 110522, https://doi.org/10.1016/j.envres.2020.110522, 2021.

Xie, F., Zhou, X., Wang, H., Gao, J., Hao, F., He, J., and Lü, C.: Heating events drive the seasonal patterns of volatile organic compounds in a typical semi-arid city, Sci. Total Environ., 788, 147781, https://doi.org/10.1016/j.scitotenv.2021.147781, 2021.

Xu, L., Duan, F., He, K., Ma, Y., Zhu, L., Zheng, Y., Huang, T., Kimoto, T., Ma, T., Li, H., Ye, S., Yang, S., Sun, Z., and Xu, B.: Characteristics of the secondary water-soluble ions in a typical autumn haze in Beijing, Environ. Pollut., 227, 296-305, https://doi.org/10.1016/j.envpol.2017.04.076, 2017.

Yang, Y., Liu, X., Qu, Y., Wang, J., An, J., Zhang, Y., and Zhang, F.: Formation mechanism of continuous extreme haze episodes in the megacity Beijing, China, in January 2013, Atmos. Res., 155, 192-203, https://doi.org/10.1016/j.atmosres.2014.11.023, 2015.

Zhang, Q., Ma, X., Tie, X., Huang, M., and Zhao, C.: Vertical distributions of aerosols under different weather conditions: Analysis of in-situ aircraft measurements in Beijing, China, Atmos. Environ., 43, 5526-5535, https://doi.org/10.1016/j.atmosenv.2009.05.037, 2009.

Zhang, Q., Quan, J., Tie, X., Li, X., Liu, Q., Gao, Y., and Zhao, D.: Effects of meteorology and secondary particle formation on visibility during heavy haze events in Beijing, China, Sci. Total Environ., 502, 578-584, https://doi.org/10.1016/j.scitotenv.2014.09.079, 2015.

Zheng, B., Zhang, Q., Zhang, Y., He, K., Wang, K., Zheng, G., Duan, F., Ma, Y., and Kimoto, T.: Heterogeneous chemistry: a mechanism missing in current models to explain secondary inorganic aerosol formation during the January 2013 haze episode in North China, Atmos. Chem. Phys., 15, 2031-2049, 2015.

Zhou, H., Lü, C., He, J., Gao, M., Zhao, B., Ren, L., Zhang, L., Fan, Q., Liu, T., He, Z., Dudagula, Zhou, B., Liu, H., and Zhang, Y.: Stoichiometry of water-soluble ions in $PM_{2.5}$: Application in source apportionment for a typical industrial city in semi-arid region, Northwest China, Atmos. Res., 204, 149-160, https://doi.org/10.1016/j.atmosres.2018.01.017, 2018.